To cite this document:
F. Ciardo, B. Lecampion, Effect of dilatancy on the transition from aseismic to seismic slip due to fluid injection in a fault, *J. Geophysical Res. - Solid Earth*, (2019)
https://doi.org/10.1029/2018JB016636

Submitted on 30 August 2018, revised 12 February 2019, accepted 6 March 2019.

Effect of dilatancy on the transition from aseismic to seismic slip due to fluid injection in a fault

F. Ciardo and B. Lecampion*

Geo-Energy Laboratory, Gaznat chair on Geo-Energy,

École Polytechnique Fédérale de Lausanne, EPFL-ENAC-IIC-GEL, Switzerland.

Key points

- Dilatancy above a critical value cancels the nucleation of dynamic rupture for injection pressure sufficient to reach residual friction
- Dilatancy delays the onset of a dynamic rupture (if occuring) and slows down aseismic crack growth
- Fault permeability increase with slip speed-up aseismic crack growth but does not affect the critical stabilizing value of dilatancy

Abstract Aseismic crack growth upon activation of fault slip due to fluid injection may or may not lead to the nucleation of a dynamic rupture depending on in-situ conditions, frictional properties of the fault and the value of overpressure. In particular, a fault is coined as unstable if its residual frictional strength τ_r is lower than the in-situ background shear stress τ_o. We study here how fault dilatancy associated with slip affect shear crack propagation due to fluid injection. We use a planar bi-dimensional model with frictional weakening and assume that fluid flow only takes place along the fault (impermeable rock / immature fault). Dilatancy induces an undrained pore-pressure drop locally strengthening the fault. We introduce an undrained residual fault shear strength τ_r^u (function of dilatancy) and show theoretically that under the assumption of small scale yielding, an otherwise unstable fault ($\tau_r < \tau_o$) is stabilized when τ_r^u is larger than τ_o. We numerically solve the complete coupled hydro-mechanical problem and confirm this theoretical estimate. It is important to note that the undrained residual strength is fully activated only if residual friction is reached. Dilatancy stabilizes an otherwise unstable fault if the nucleation of an unabated dynamic rupture -without dilatancy- is affected by residual friction, which is the case for sufficiently large injection pressure. We also discuss the effect of fault permeability increase due to slip. Our numerical results show that permeability increases lead to faster aseismic growth but do not impact the stabilizing effect of dilatancy with respect to dynamic rupture.

1 Introduction

Seismic and aseismic ruptures associated with anthropogenic fluid injection at depth have been observed in variety of settings (Healy et al. 1968, Hamilton and Meehan 1971, Scotti and Cornet 1994, Cornet et al. 1997, Shapiro et al. 2006, Ellsworth 2013, Skoumal et al. 2015, Bao and Eaton 2016) to cite a few. Industrial

*Corresponding author: Brice.Lecampion@epfl.ch

applications involved range from waste water disposal to the stimulation of enhanced geothermal systems and hydraulic fracturing.

Injection of fluid into the sub-surface alters the local stress state. Pre-existing fractures/faults or intact rock mass can fail due to the local reduction of effective stresses associated with pore pressure increase. Shear fractures can thus be activated and propagate along favorably oriented planes of weaknesses/faults. In some cases, the aseismic slip may lead to the nucleation of a dynamic rupture (seismic event). A necessary ingredient for such a transition from aseismic to seismic slip is the reduction of fault frictional strength with slip, i.e. when the frictional resistance decreases faster than the elastic unloading associated with slip (Cornet 2015).

The transition from the activation of aseismic slip to the nucleation of a seismic event due to fluid injection has been discussed theoretically (Garagash and Germanovich 2012) and observed in-situ (Scotti and Cornet 1994, Cornet et al. 1997, Guglielmini et al. 2015, Wei et al. 2015, Cornet 2016). We investigate here the effect of fault/fracture dilatancy associated with slip on the transition from aseismic crack propagation to seismic slip in the context of fluid injection. The physical mechanism of dilatancy associated with sliding over fault's asperities leads to a pore pressure drop under undrained conditions and thus to a fault strengthening denoted as dilatant hardening (Segall and Rice 1995, Segall et al. 2010, Rudnicki and Chen 1988). Strong dilatant behavior has been observed during aseismic crack propagation in scaled laboratory experiments by Lockner and Byerlee (1994), Samuelson et al. (2009) and inferred during field experiment of the stimulation of geothermal reservoir (Batchelor and Stubs 1985) suggesting that dilatancy possibly plays an important role on shear fracture propagation in some cases.

Although the concept of dilatant hardening associated with undrained conditions has been studied on saturated rock masses (Rice 1975) as well as on frictional weakening faults loaded by tectonic strain (Rudnicki, J. W. 1979, Segall and Rice 1995, Shibazaki 2005, Segall et al. 2010), the quantification of its effect on the transition from aseismic to seismic slip propagation in association with fluid injection remains elusive.

The interplay between fluid injection, in-situ conditions, frictional properties and evolution of the hydraulic properties of fault present a highly coupled problem leading to a wide range of possible behavior even under 'simple' homogeneous in-situ conditions (Garagash and Germanovich 2012, Viesca and Rice 2012, Zhang et al. 2005). In this paper, we extend previous work to account for fault dilatancy and quantify its impact on the propagation of a shear crack induced by a constant pressure injection. For simplicity, we reduce to a 2D configuration and model the fault / joint as a planar thin strip where both shear slip and fluid flow are localized. We adopt a simple linear weakening slip-dependent friction law Ida (1972) combined with a non-associated flow rule to account for dilatancy, assume isothermal conditions and neglect poroealastic stress changes in the surrounding rock. We pay particular attention to the verification of our numerical solver and discuss the different type of crack propagation (aseismic/seismic) as a function of in-situ and injection conditions. We also put in perspective our results at the light of theoretical arguments under the small-scale yielding approximation (Rice 1968, Palmer and Rice 1973).

2 Problem formulation

We consider an infinite planar fault in an infinite homogeneous isotropic elastic medium (see Figure 1) under plane-strain conditions. We also assume that the host rock has a much lower permeability than the fault. As a result, the fluid flow only occurs along the fault plane from a source injection located at the middle of the fault in the 2D space - more precisely a line-source in the out-of-plane direction to satisfy plane-strain conditions. Furthermore, we assume an uniform initial in-situ stress and pore pressure field prior to the start of the injection.

Such a homogeneous model is obviously only valid for small fault slippage length compared to the background in-situ gradient but it allows to isolate and understand the different type of responses in a clearer way. Although different type of injection conditions, either away or directly on the fault, can be investigated, we restrict here to the case of a constant pressure injection from a point source directly in the fault.

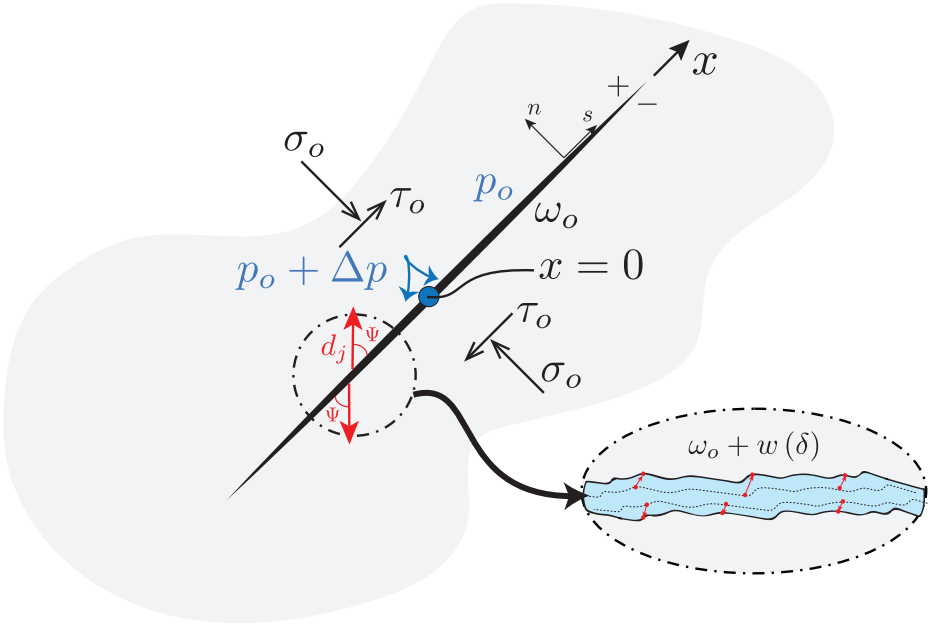

Figure 1: Model of frictional weakening dilatant fault & loading conditions. Zoom represents schematically the dilatant process that occur during shear fracture propagation.

2.1 Equilibrium, activation and dilatancy of slip-weakening fault

We consider the occurrence of a mode II shear crack of length $2a$ on the fault plane due to a constant pressure fluid injection. Initially, we assume the fault to be in static equilibrium with the uniform in-situ stress state. Upon activation of slip due to the increase of fluid pressure along the fault, the bi-dimensional quasi-static elastic equilibrium can be written as the following integral equations relating fault tractions and displacement discontinuities in the local normal and tangential frame along the fault plane (using the convention of summation on repeated indices):

$$t_i(x,t) = t_i^o(x) + \int_{-a}^{a} K_{ij}(\xi,x) d_j(\xi,t) \mathrm{d}\xi, \text{ for } i,\, j = n,\, s \tag{1}$$

where $t_i = \sigma_{ij} n_j$ is the current traction vector acting along the fault, t_i^o its value under the initial in-situ stress and d_j denotes the vector of displacement discontinuities on the fault:

$$d_j = u_j^+ - u_j^- \tag{2}$$

The quasi-static fundamental elastic displacement-discontinuity tensor K_{ij} is known in closed-form for a bi-dimensional infinite medium (see e.g. Gebbia (1891), Crouch and Starfield (1983), Hill et al. (1996)). It is worthwhile to recall that for a planar crack, the shear and normal boundary integration uncouples as $K_{sn} = K_{ns} = 0$. As a result, shear slip does not induce any changes in the normal stress along the planar fault. However, if shear slip induces plastic dilatancy, the corresponding normal displacement discontinuity associated

with dilatancy modify the normal stress along the fault. We note that the use of a quasi-static approach will obviously overshoot any finite dynamic rupture. Although a quasi-dynamic approximation (Rice 1993) would provide more realistic results without the expense of a complete dynamic simulation, we restrict our-self mostly to the nucleation of a dynamic rupture for which a quasi-static approximation is granted.

We adopt the convention of normal stresses positive in compression. The normal and shear components of the traction vector on the fault plane $t_i = (t_n, t_s)$ (in the local $s - n$ reference system on Figure 1) will be noted as $\sigma = -t_n = -(n_i \sigma_{ij} n_j)$ and $\tau = s_i \sigma_{ij} n_j$ for the normal and shear component respectively. We will also write the normal displacement discontinuities as $d_n = w$ (positive for opening) and the shear displacement discontinuities (slip) as $d_s = \delta$ (positive in a clockwise rotation).

2.1.1 Activation and plasticity

We assume that the fault obeys a Mohr-Coulomb yield criterion without cohesion, accounting for a slip weakening of friction. The yield criterion is:

$$F(\tau, \sigma') = |\tau| - f(\delta)\sigma' \leq 0, \tag{3}$$

where $f(\delta) = \tan(\phi(\delta))$ is the friction coefficient (ϕ the corresponding friction angle), which is supposed to weaken linearly with slip δ, from a peak value f_p to a residual value f_r for slip larger than δ_r (see Figure 2-bottom-left). $\sigma' = \sigma - p(x,t) > 0$ is the local effective normal stress acting on the fault plane. We will write the initial in-situ conditions (prior to fluid injection) as $\sigma'_o = \sigma_o - p_o$ and τ_o for the ambient effective normal stress and shear stress respectively.

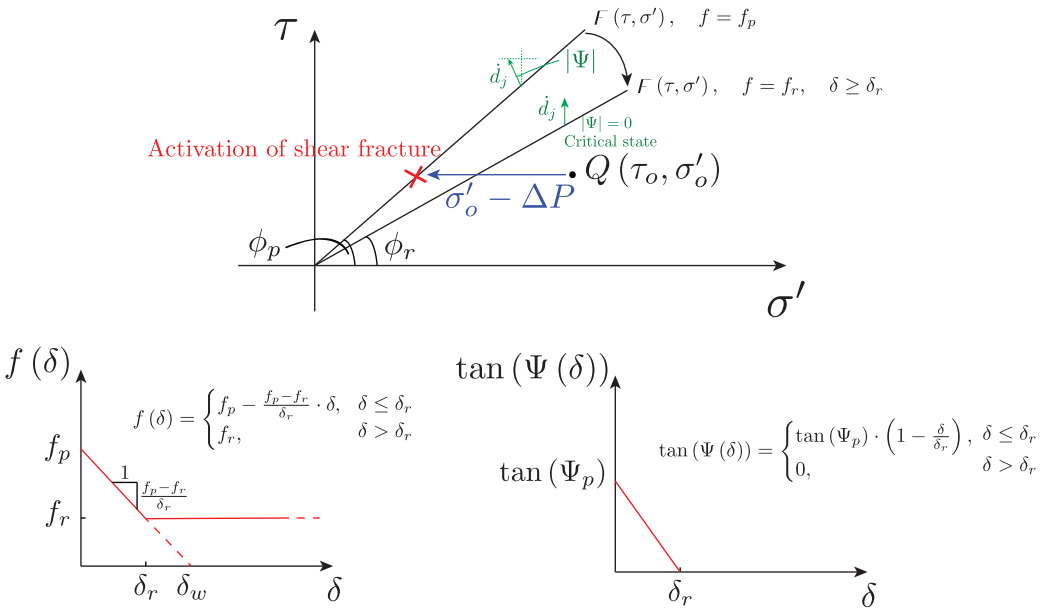

Figure 2: The Mohr-Coulomb plot (top) illustrates the evolution of the yielding surface $F(\tau, \sigma')$ with weakening of friction coefficient as well as the evolution of plastic displacement discontinuity vector $\dot{d}_j$ with slip after shear fracture activation due to fluid over-pressure ΔP. The linear evolution of friction coefficient $f = \tan(\phi)$ (left) and dilatancy angle $\tan(\psi)$ (right) with slip δ are displayed in the bottom plots.

The fault is activated when the injection overpressure is sufficient to reach the Mohr-Coulomb criterion at peak initial friction (see Figure 2-top), and shear slip starts to occur on the fault. We model the fault

as rigid plastic and account for a possible dilatant behavior. Using a non-associative flow rule, the rate of displacement discontinuities (denoted with a dot) derive from a plastic potential function of the corresponding effective tractions when the yield criterion is satisfied (i.e. $F = 0$):

$$\dot{d}_i = \lambda \frac{\partial G}{\partial t'_i} \tag{4}$$

The (scalar) plastic multiplier λ is either greater than zero as long as the local stress state satisfies the Mohr-Coulomb yield criterion (3), or equals to zero for non-yielded stress state (for which $F(\tau, \sigma') < 0$ and the fault is not activated). Plastic slip takes place along the yielding surface (see plastic strain vector in Figure 2-top). This can be summarized by the following set of conditions (Lubliner, J. 2005, Maier et al. 1993):

$$\lambda \geq 0, \quad F(\tau, \sigma') \leq 0, \quad \lambda F(\tau, \sigma') = 0 \tag{5}$$

In order for plastic flow to occur, the tractions on the fault must persist on the yield surface $F = 0$, while upon unloading plastic flow stops as soon as $F < 0$. This requirement is often denoted as a consistency condition and written as

$$\lambda \dot{F}(\tau, \sigma') = 0, \quad (\text{if} \quad F(\tau, \sigma') = 0) \tag{6}$$

It allows to obtain the plastic multiplier λ (see e.g. (Lubliner, J. 2005, Simo and Hughes 1997) for more details).

We use a non-associated Mohr-Coulomb criterion with a dilatancy angle ψ decreasing with accumulated slip δ. We write the plastic potential as

$$G(\tau, \sigma'_n) = |\tau| - \tan(\psi(\delta))\, \sigma' \tag{7}$$

As a result, the rate of slip and opening displacement discontinuity are related to each other as:

$$\dot{d}_s = \dot{\delta} = \lambda \text{sign}(\tau) \tag{8}$$

$$\dot{d}_n = \dot{w} = \lambda \tan(\psi(\delta)) \tag{9}$$

We assume that the dilatancy coefficient (tangent of the dilatancy angle ψ) decreases linearly with slip from an initial peak value $\tan\psi_p$ to zero: the fault is assumed to reach a critical state (where the dilatancy angle is zero) over the same slipping distance δ_r at which it reaches residual friction (see Figure 2-bottom-right). Such a choice is consistent with experimental observations that a critical state (where no change of volume occur) is reached after sufficient plastic deformation for most rocks and granular material. Integration of (8)-(9) provides the following quadratic evolution of fracture width due to the dilatancy induced by slip:

$$w(\delta) = \int_0^{\delta} \tan(\psi(\delta'))\, \mathrm{d}\delta' = \begin{cases} 2\Delta w \left(\frac{\delta}{\delta_r}\right) - \Delta w \left(\frac{\delta}{\delta_r}\right)^2 & \delta < \delta_r \\ \Delta w & \delta > \delta_r \end{cases} \tag{10}$$

where Δw denotes here the maximal / final dilatant opening at residual friction:

$$\Delta w = \int_0^{\delta_r} \tan(\psi(\delta'))\, \mathrm{d}\delta' = \tan(\psi_p)\, \frac{\delta_r}{2} \tag{11}$$

A similar law for the dilatancy evolution with frictional slip has been proposed by Rudnicki and Chen (1988) to model uplift in sliding over asperities of a long homogeneous slab subjected to shear and normal mechanical loadings. Initially, the fault is supposed to have a constant uniform 'hydraulic aperture' ω_o which can be considered as the fault gouge thickness in such a model. The ratio between the maximal dilatant increment of fracture width Δw and this initial aperture ω_o defines a dilatant strain $\epsilon_d = \dfrac{\Delta w}{\omega_o}$ which can be related to the

maximum change of fault porosity due to slip. Such a quantity will directly appear in the hydro-mechanical coupling.

Dilatancy is known to be function of effective normal stress - with lower dilatancy angle typically measured under larger confinement (Matsuki et al. 2010, Barton et al. 1985). Measured value of the peak dilatancy angle (at small slip) ranges from $\sim 40^\circ$ at 5 MPa of confinement to $\sim 6^\circ$ at 30 MPa for Inada granite (Matsuki et al. 2010), leading to values of ϵ_d in a range of $10^{-3} - 10^{-2}$. Laboratory experiments on quartz fault gouge (Samuelson et al. 2009) provides value of ϵ_d in the range $10^{-4} - 10^{-3}$ at effective confinement up to 20 MPa, values which appears of similar order than the one measured at larger confinement (Marone et al. 1990).

In what follows, for sake of simplicity, we do not explicitly account for the complete details of the dependence of dilatancy with normal effective stresses. The peak dilatancy angle can be implicitly taken to be a function of the level of in-situ confinement prior to injection. Moreover, we acknowledge that a relatively large range of possible value of the dilatant strain ϵ_d may exist from 10^{-4} to 10^{-2}.

2.1.2 Slip weakening and nucleation length-scale

Following Uenishi and Rice (2003), Garagash and Germanovich (2012), we introduce a characteristic nucleation patch length-scale a_w

$$a_w = \frac{E'}{2\tau_p}\delta_w \tag{12}$$

to scale the crack length. This characteristic nucleation length-scale is obtained by normalizing the slip δ and shear stress τ in the elasticity equation (1) by $\delta_w = \dfrac{f_p}{f_p - f_r}\delta_r$ and $\tau_p = f_p\sigma'_o$, respectively. δ_w denotes the amount of slip at which the friction coefficient goes to zero if an unlimited linear slip-weakening friction law is considered (see Figure 2-bottom-left). Typically δ_w is of the order the fault's asperities and thus ranges between 0.1 mm to 10 mm. $\tau_p = f_p\sigma'_o$ defines the peak frictional strength at ambient conditions, its difference from the ambient shear stress τ_o quantify the fault stress criticality. Such a peak fault shear strength can vary widely with depth, fault orientation as well as hydrogeological conditions (normally pressurized versus over-pressured formations) and thus can range between a fraction to hundred of MegaPascals. We thus deduce that the range of characteristic patch length-scale a_w (e.g. for a crystalline rock with $\mathrm{E}' \sim 60$ GPa) can approximately ranges between tens of centimeters to tens of meters depending on geological conditions.

2.2 Fluid flow

Under the assumption of much smaller rock permeability compared to the longitudinal fault permeability, the fluid flow is confined within the fault zone. This case corresponds to an immature fault with little accumulated slip for which the extent of the damage zones around the fault core remains limited. For active and mature fault, the permeability structure around the fault can not be neglected. Much larger permeabilities have indeed been measured in the damage zone (that can have decameters thickness) of active mature fault compared to the fault gouge unit (Lockner et al. 1999). Here, we restrict to the case of an immature / young fault for which the flow is confined in the gouge. Such a hypothesis could also be valid for inactive mature fault that would have exhibited a plugging of their damage zone permeability (e.g. via long term thermo-hydro-chemical effects).

The mass balance equation width-averaged across the fault hydraulic aperture w_h of the gouge layer thus reduces to:

$$\frac{\partial \rho w_h}{\partial t} + \frac{\partial \rho w_h V}{\partial x} = 0, \tag{13}$$

where ρ is the fluid density and V is the averaged fluid velocity. The fault hydraulic aperture $w_h = \omega_o + w(\delta)$ is the sum of its initial value ω_o and the additional dilatant aperture function of slip (see eq. (10)).

By combining fluid compressibility (taken as liquid water) and pore compressibility of the fault gouge in an unique parameter β $\left[M^{-1}TL^2\right]$, the width averaged fluid mass conservation (13) along the fault (x-axis) reduces to

$$w_h\beta\frac{\partial p}{\partial t} + \tan(\psi(\delta))\frac{\partial \delta}{\partial t} + \frac{\partial q}{\partial x} = 0, \tag{14}$$

where $q = w_h V$ is the uni-dimensional local fluid flux given by Darcy's law:

$$q = -\frac{w_h k_f(\delta)}{\mu}\frac{\partial p}{\partial x}, \tag{15}$$

with μ the fluid viscosity $\left[ML^{-1}T^{-1}\right]$ and $k_f(\delta)$ the fault intrinsic permeability $\left[L^2\right]$. The hydraulic diffusivity of the fault α $\left[L^2/T\right]$ is defined as:

$$\alpha = \frac{k_f}{\mu\beta} \tag{16}$$

In particular, the location of the fluid / pressure front evolves as $\sqrt{4\alpha t}$ for such type of diffusion problem (Carslaw and Jaeger 1959).

In conjunction with the increase of the fault aperture with dilatant slip (10), the longitudinal fault permeability may also evolve with shear slip. A number of different models have been proposed in the literature for the evolution of permeability with slip, from using the cubic law for the fault transmissivity (product of permeability $k_f = w_h^2/12$ and hydraulic aperture w_h), to an exponential dependence of permeability with normal stress, or Cozeny-Karman type relations. Here, we first make the assumption of a constant fault permeability $k_f = \omega_o^2/12$ before relaxing such an approximation in section 6 in order to properly gauge its effect.

It is important to note that even in the absence of permeability evolution, the changes of hydraulic aperture induced by dilatancy still impact the fluid flow in a non-trivial and non-linear way. This is notably due to the sink term $\tan(\psi(\delta))\frac{\partial \delta}{\partial t}$ associated with slip induced dilatancy. Fluid flow can not be uncoupled from mechanical equilibrium and fault slip, contrary to the case of zero dilatancy (Garagash and Germanovich 2012), where for a constant pressure injection ΔP, the pore pressure on the fault plane is simply given by $p(x,t) = p_o + \Delta P \mathrm{Erfc}\left|\frac{x}{\sqrt{4\alpha t}}\right|$. No simple analytical solution does exist for this complete non-linear hydro-mechanical coupling.

The effect of slip induced dilatancy leads to a pore-pressure drop under undrained conditions (denoted here as Δp_u). At large slip rate, the change of hydraulic width from its initial value up to its maximum value $\omega_o + \Delta w$ (11) will be sudden. In such an undrained limit the fluid has no time to flow and the associated pore pressure change can be directly obtained from mass conservation (14):

$$\Delta p_u = -\frac{\Delta w}{\omega_o \beta} = -\frac{\epsilon_d}{\beta} \tag{17}$$

This undrained pore-pressure drop will be localized at the crack tips, where frictional slip weakening occurs. From the previously discussed range of the dilatant strain $\epsilon_d \in [10^{-4} - 10^{-2}]$, for a compressibility coefficient β between the one of liquid water and usual pore compressibility ($\beta \in [5 - 100]\, 10^{-10}\mathrm{Pa}^{-1}$), we obtain a range of values $[0.01 - 20]$ MPa for such an undrained pore-pressure drop. The previous estimate corresponds to the maximum possible amount of undrained pore-pressure drop (sudden slip from zero to δ_r). A re-strengthening of the fault is thus expected as the effective normal stress increase locally as a result of this undrained pore-pressure drop. Similar dilatant hardening is typically observed in fluid-saturated porous medium subject to undrained loading (Rice 1975, Rudnicki, J. W. 1979). It is important to underline that such re-strengthening effect is less pronounced for "mature" faults, for which pore fluid diffusion normal to fault plane (across the permeable units of damaged zone) may prevail against fluid diffusion along the fault gouge unit.

2.3 Initial and injection conditions

Initially, the (peak) fault strength $\tau_p = f_p \sigma'_o$ at ambient condition is everywhere larger than the in-situ shear traction on the fault τ_o. In other words, the fault is initially stable (i.e. $F(\tau_o, \sigma'_o) < 0$) and locked before the start of fluid injection. We consider here the case of a constant over-pressure ΔP at the injection point:

$$p(x = 0, t) = p_o + \Delta P, \tag{18}$$

We assume that the choice of the injection over-pressure ΔP is such that the minimum principal effective stress σ'_n always remain compressive (positive) such that no hydraulic fracture type failure occurs: i.e. $\Delta P < \sigma'_o$. A constraint often enforced in practice for large scale injection but also sometimes during hydraulic stimulation of geothermal reservoirs. We investigate here the activation of a shear crack that would occur if the overpressure ΔP at the injection point is sufficient to lower the effective normal stress and reach Mohr-Coulomb failure. Such a minimum over-pressure ΔP for activation is directly related to the fault criticality:

$$\frac{\Delta P}{\sigma'_o} \geq 1 - \frac{\tau_o}{\tau_p} \tag{19}$$

The ratio τ_o/τ_p represents the stress criticality of the fault at ambient condition (quantifying how far the fault is from failure). For a critically stressed fault ($\tau_o/\tau_p \sim 1$), slip is activated for small over-pressure. On the other hand, a fault whose initial uniform stress state is much lower than its peak frictional strength ($\tau_o/\tau_p \ll 1$) requires a larger over-pressure to activate a shear crack, and is sometimes referred to as a marginally pressurized fault.

3 Activation and transition between aseismic and seismic slip

3.1 Case of a non-dilatant fault

We first briefly recall the results obtained for the case of a non-dilatant fault by Garagash and Germanovich (2012) using the the same linear frictional weakening model. This summary is required in order to properly put in perspective the effect of a dilatant fault behavior.

After activation of aseismic slip, there exist two ultimate fault stability behaviors depending on the relative value of the residual strength (defined at ambient condition) $\tau_r = f_r \sigma'_o$ compared to the in-situ background shear stress τ_o. Notably, if the residual frictional strength τ_r exceeds the ambient shear stress τ_o, the fault is *ultimately stable*. On the other hand, for a residual frictional strength τ_r lower than τ_o, the fault is unstable. Figure 3 summarizes the different behaviors, as a function of the dimensionless fluid over-pressure $\Delta P/\sigma'_o$, stress criticality τ_o/τ_p and relative value of τ_r with respect to the initial shear stress τ_o. Region 1 on Figure 3 corresponds to the trivial case of an injection without activation of any slip.

For an ultimately stable fault (for which the residual strength τ_r is larger than the ambient shear stress τ_o), it can be shown that for an over-pressure sufficient to activate slip, at large time / large crack length the shear crack grows quasi-statically (aseismically) as long as the fluid injection continues (regions 2 and 3 on Figure 3). However, because of the weakening of its frictional properties, an ultimately stable fault may host an episode of seismic slip followed by an arrest (region 2 on Figure 3). Such a 'seismic event' depends on both the stress-criticality and the amount of over-pressure. For a moderate over-pressure (sufficient to activate slip), the shear-crack first lags behind the fluid diffusion front and, due to the interplay between fluid pressurization and frictional weakening, a dynamic event nucleate and grows until it catches up the fluid pressure diffusion front ahead of which the over-pressure is minimal. The subsequent propagation is then a-seismic and tracks the fluid

front as long as injection continues. In other words, depending on the value of fluid over-pressure applied in the middle of the fault, the local accumulation of slip during the (aseismic) crack propagation varies. If the fluid over-pressure induces a large local slip accumulation during the aseismic propagation (such that it exceeds the residual slip δ_r), the fault never exhibits a dynamic event (strictly aseismic propagation - region 3), otherwise a nucleation of a dynamic rupture episode occurs (region 2 in Figure 3) .

The situation is different for unstable fault ($\tau_r < \tau_o$) - regions 4a, b, c on Figure 3. It can be proved that an unabated dynamic rupture will always occur when $\tau_r < \tau_o$. The nucleation length (and time of nucleation) depends again on stress criticality, the value of over-pressure and in some cases (region 4c) on the value of the residual friction f_r. For criticality stress fault (region 4a - $\tau_o/\tau_p \sim 1$), the nucleation patch size a_c is independent of the overpressure $a_c = 0.579\, a_w$ (Garagash and Germanovich 2012). In these cases, even a small over-pressure is sufficient to nucleate a dynamic rupture and the fluid front lies well within the crack when the unabated instability occurs. For unstable but marginally pressurized fault (moderate stress criticality), subjected to a moderate value of over-pressure, a transient seismic event may occur and then arrest when the crack front catches up with the fluid front. However, here (region 4b in Figure 3) a re-nucleation always occurs (affected by residual friction) leading then to an unabated dynamic rupture. For larger of over-pressure, a single nucleation of an unabated dynamic rupture occur (region 4c).

3.2 Effect of dilatancy

3.2.1 Undrained fault response

At high slip rate, the undrained response associated with dilatancy causes a pore-pressure drop (17). Scaling the fluid pressure by effective normal in-situ stress, we express the undrained response via the following dimensionless undrained pressure change

$$\frac{\Delta p_u}{\sigma'_o} = -\frac{\epsilon_d}{\beta \sigma'_o} \tag{20}$$

The dimensionless ratio $\frac{\epsilon_d}{\beta \sigma'_o}$ quantifies the effect of dilatancy in terms of pore pressure drop under undrained conditions with respect to the initial confining stress. For a realistic range of effective in-situ normal stress of [1-200] MPa, whose extremes may represent the case of normally pressurized and over-pressurized fault located approximately between 0.1 and 5 Km below the Earth's surface, and for the previously reported range for undrained pore-pressure drop ϵ_d/β, the dimensionless dilatancy parameter $\frac{\epsilon_d}{\beta \sigma'_o}$ ranges between 0.01 (deeper conditions/low dilatancy) and 20 (shallow conditions / large dilatancy).

Dilatancy is mobilized in the frictional weakening zone. Moreover, it's impact on pore-pressure is modulated by the slip rate $\partial\delta/\partial t$ (see eq. 14). In proximity of a dynamic event when the slip rate increases rapidly, the undrained pore pressure drop leads to a local strengthening at the crack tip (dilatant hardening). In the case where the slip rate and crack velocity is larger than the fluid flux, the undrained dilatant pore-pressure drops will be at its maximum (17) and will persist inside the crack away from the crack tip. We can thus quantify the associated strengthening by adding its effect to the fault residual strength - defining an undrained residual shear strength τ_r^u as:

$$\tau_r^u = \tau_r - f_r \Delta p_u = \tau_r \left(1 + \frac{\epsilon_d}{\beta \sigma'_o}\right) \tag{21}$$

From the ranges of value previously discussed, we see that the undrained shear strength can be from 1.01 to 2 times larger than the drained residual strength.

On the other hand, the shear-induced dilation impact (via the non-associated flow rule (9)) the distribution of normal stress along the fault through the effect of corresponding opening displacement discontinuity in the

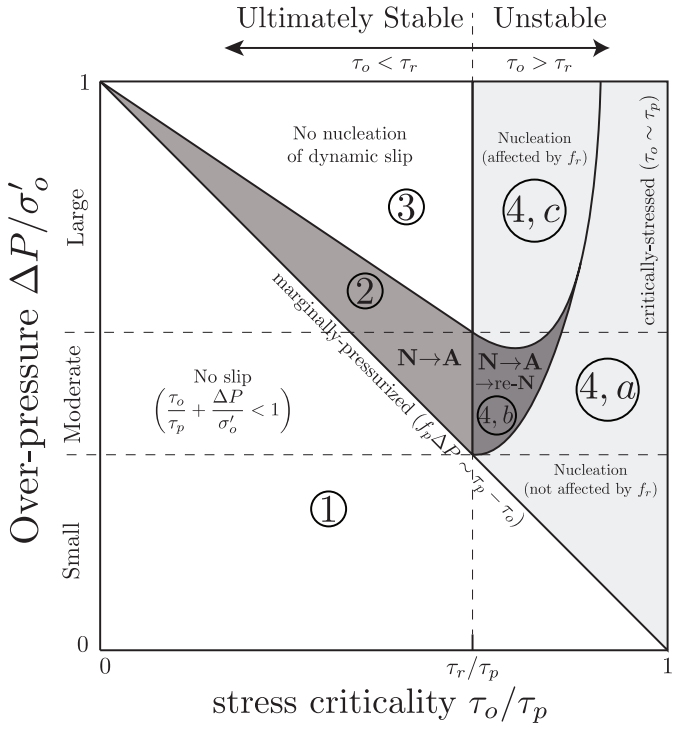

Figure 3: Phase diagram of (Garagash and Germanovich 2012) that describes the different regimes of propagation for a non-dilatant fault, as a function of the dimensionless fluid over-pressure $\Delta P/\sigma'_o$ and stress criticality τ_o/τ_p. Region 1 corresponds to the trivial case of an injection without fault re-activation. Regions $4a$, b, c corresponds to the unstable fault case for which an unabated dynamic rupture occurs as the residual shear strength (defined at ambient conditions) is lower than the in-situ shear stress ($\tau_r < \tau_o$). Regions 2 and 3 corresponds to the case of ultimately stable faults ($\tau_r > \tau_o$) for which most of the crack growth is aseismic although transient seismic slip may occur (region 2).

elasticity equation (1). Inside the crack, the opening of the fault leads to an increase of compressive normal stress, whereas ahead the crack tips it induces tensile stresses therefore reducing the fault frictional strength. There is thus an interplay between the non-local stress-induced perturbation due to fault opening and dilatant hardening. The tensile stresses ahead of the tip have however a lower magnitude than the undrained pore-pressure drop. For instance, if we suppose that the weakening region is small compared to the whole crack size (small scale yielding conditions), the mechanical opening is uniform and equal to Δw along the whole crack. We can thus estimate the tensile normal stress ahead of the crack front using the solution for an edge dislocation (e.g. (Hill et al. 1996)) of intensity Δw. Scaling the distance $\hat{x}$ from the dislocation by the nucleation lengthscale a_w, we have

$$\Delta\sigma = -\frac{E'}{4\pi a_w}\frac{\Delta w}{\hat{x}/a_w} \tag{22}$$

The corresponding stress intensity for such a singular field is thus $E'\Delta w/(4\pi a_w)$. For a maximum increment of dilatant width Δw of the order of few millimeters and corresponding estimate of the nucleation patch size a_w gives an order of magnitude of about $\sim$ 1 MPa or less for such stress perturbation. Taking the ratio of such stress intensity with the estimate of the undrained pore-pressure drop (17), after re-arranging, one obtain $E'\beta\omega_o/(4\pi a_w)$ which will be always smaller than one as $E'\beta \simeq O(10)$ and $\omega_o/a_w \simeq O(10^{-2})$. We therefore conclude that the mechanical effect of dilatancy induced tensile stresses ahead of the crack tip is lower than the undrained pore pressure change Δp_u. The dilatant hardening effect dominates. This is confirmed by our fully coupled numerical simulations (see section 5).

3.2.2 Small scale yielding & stability condition

Following the work of Garagash and Germanovich (2012), we extend their ultimate stability condition to account for the effect of dilatant hardening. This stability condition can be obtained under the assumption of small scale yielding (s.s.y) which holds when the shear crack of half-length a is sufficiently larger than the characteristic length scale a_w such that all the frictional weakening occurs in a small zone near the crack tip. Such a localization of the frictional weakening in a small zone near the crack tip can be observed on our numerical results (see section 5.1). Under such assumption, the fracture energy G_c (Rice 1968, Palmer and Rice 1973) for the linear frictional weakening model can be estimated as:

$$G_c = \int_0^{\delta} \tau(\delta) - \tau_r \, \mathrm{d}\delta \simeq \frac{\delta_r}{2}(f_p - f_r) \times \sigma'(a) \tag{23}$$

under the assumption that the effective normal stress $\sigma'(a)$ is constant within the weakening region. The condition for quasi-static crack growth of such a shear crack reduces to the classical linear elastic fracture mechanics criteria. The driving force for propagation G (the energy release rate) must equal G_c for quasi-static growth to occur. A criteria which for such a shear crack reduce to:

$$G = \frac{K_{II}^2}{E'} = G_c, \tag{24}$$

where K_{II} is the stress intensity factor for the given loading and crack size.

As all the crack -besides the small weakening zone at the tips- is at residual frictional strength, the stress intensity factor can be obtained by superposition of the effect of the loading of the crack by i) the residual frictional strength at ambient condition $\tau_r = f_r\sigma'_o$ minus the far-field in-situ shear stress τ_o (which are both uniform along the crack) and ii) the effect of the over-pressure due to the fluid injection on the decrease of shear strength $f_r\Delta p(x,t)$. The stress intensity factor for such a configuration is thus given as (Rice 1968, Tada et al.

2000)

$$K_{II} = (\tau_o - \tau_r)\sqrt{\pi a} + \underbrace{f_r \sqrt{\frac{a}{\pi}} \int_{-a}^{+a} \frac{\Delta p\,(x,t)}{\sqrt{a^2 - x^2}} \mathrm{d}x}_{\Delta K_{II}(a,t)} \tag{25}$$

On the contrary to the non-dilatant case, the exact solution for the over-pressure $\Delta p\,(x,t)$ evolution along the fault is not known analytically. It is the complete solution of the coupled hydro-mechanical problem in the dilatant case. However, in order to obtain an ultimate stability condition for large crack length, it can be approximated as follow. If the shear crack a is much larger than both the slipping patch length scale a_w (which is required for the s.s.y approximation to be valid) and the diffusion length scale $\sqrt{4\alpha t}$, the over-pressure can be approximated as the sum of a point source term of intensity ΔP for the effect of the injection (as $a \gg \sqrt{4\alpha t}$) and the response of the undrained pore-pressure drop. Moreover, if the crack velocity is much larger than the fluid velocity - which would be true in all cases if the crack accelerates - the undrained pore-pressure drop can be assumed to remain constant and equal to Δp_u (eq. (17)) over the entire crack. Under those conditions, the stress intensity factor reduces to:

$$\begin{aligned} K_{II} &\simeq (\tau_o - \tau_r)\sqrt{\pi a} + \frac{f_r \Delta P}{\sqrt{\pi a}} + \frac{\tau_r \Delta p_u}{\sigma'_o}\sqrt{\pi a} \\ &\simeq (\tau_o - \tau_r^u)\sqrt{\pi a} + f_r \frac{\Delta P}{\sqrt{\pi a}} \end{aligned} \tag{26}$$

where the undrained shear strength previously introduced appear. This expression is strictly similar to the one derived in Garagash and Germanovich (2012) pending the replacement of the residual shear strength τ_r by its undrained counterpart $\tau_r^u = \tau_r(1 + \epsilon_d/(\beta\sigma'_o))$ (21). As previously anticipated the effect of dilatancy is akin to an increase of the residual shear strength.

The reasoning of Garagash and Germanovich (2012) for the ultimate stability can thus be directly transposed to the dilatant case. In the limit of infinitely large crack $a \to \infty$, one directly see that the stress intensity factor tends to either $+\infty$ if $\tau^o > \tau_r^u$ and $-\infty$ if $\tau^o < \tau_r^u$. In other words, if the initial shear stress τ^o is larger than the undrained residual strength, the fault is ultimately unstable as the stress intensity factor diverges for large crack length: the nucleation of a dynamic rupture will thus always appear. On the other hand, the fault is ultimately stable when $\tau^o < \tau_r^u$. We therefore see that as the undrained residual shear strength τ_r^u is larger than τ_r, sufficient dilatancy may stabilize a fault that otherwise would be unstable. The minimal/critical amount of dilatancy ϵ_d^c required for such a stabilization to occur is simply given as:

$$\epsilon_d^c = \beta\sigma'_o \left(\frac{\tau_o}{\tau_r} - 1\right) = \beta\sigma'_o \left(\frac{\tau_o}{\tau_p}\frac{f_p}{f_r} - 1\right) \tag{27}$$

It is interesting to note that it directly depends on the residual stress criticality τ_o/τ_r, and the in-situ effective normal stress.

It is important to note that - obviously - in the ultimately stable case ($\tau_r^u > \tau_o$) the stress intensity factor does not tend to $-\infty$ in reality as the propagation can only occur for $G = G_c$. Upon continuous fluid injection, a stable quasi-static growth will occur and will be modulated by the fluid diffusion: i.e the crack will decelerate for large crack length at constant injection. It is actually possible to devise an approximated solution for such a quasi-static growth by hypothesizing that the crack length evolves as a factor of the fluid front: $a = \gamma\sqrt{4\alpha t}$. An approximation of the pore-pressure evolution accounting for the undrained pore-pressure drop at the tip can be obtained and used in eqns. (24) and (25) to obtain an estimate of γ. Such an approximated solution is detailed and compared to our numerical results in Supporting Information. Such a refined (but still largely

approximated) solution for the pore-pressure evolution gives the exact same limit for the stability condition at large crack length as well as critical dilatancy than the simpler profile postulated previously.

To conclude, before moving to the complete numerical solution of the problem, a word of caution is required with respect to the stability condition $\tau_o < \tau_r^u$. Such a stability condition holds on the premise that most of the crack is at residual friction pending a small weakening zone (s.s.y approximation). It is valid for sufficiently large crack length compared to a_w and peak slip larger than δ_r. Only under this assumption, the maximum undrained pore-pressure (20) can be achieved. If a dynamic rupture nucleates for slip smaller than the residual δ_r, the s.s.y is invalid: the undrained pore-pressure response will not be fully activated and thus not sufficient to quench the nucleation of a dynamic rupture. However, upon reaching larger crack length (and thus residual friction), the complete undrained pore-pressure will ultimately kicks in such that a dynamic rupture should arrest if the ultimate undrained s.s.y stability condition ($\tau_r^u > \tau_o$) is satisfied.

4 Numerical scheme description

Although approximation of the complete problem have allowed to highlight the stabilizing effect of dilatancy on the nucleation of a dynamic rupture associated with fluid injection, a full numerical solution is needed to investigate the complete parametric space and test the concept of a critical dilatancy.

The complete problem described in section 2 is fully coupled due to the dilatant fault behavior as well as non-linear due to the evolution of the fault hydraulic width (even if the fault permeability remains constant). It also involves the tracking of the moving crack tips. The shear crack evolves in space and time along the fault, paced by pore pressure evolution. Equation (1), which links tractions t_i on the fault plane with displacement discontinuities d_j, evolves in time due to the moving crack domain Γ. The developed numerical scheme solve this coupled problem by determining simultaneously the plastic multipliers λ in the 'active' zone of the domain (i.e. where $F(\tau, \sigma_n') = 0$) through equations (1-8-9) and the increment of pore pressure Δp along the whole fault (through equation (14) and Darcy's law (15)).We then recompute the increment of tractions (due to both increment of slip and the associated increment of hydraulic width) along the rest of the domain via the non-local elasticity equation (1). We have chosen a backward-Euler (implicit) time integration scheme for stability and robustness. A choice that stems from the restrictive CFL condition on the time-step for diffusion problem (e.g. (Quarteroni et al. 2000)) - which even deteriorates for strong non-linear variation of permeability similar to the hydraulic fracturing case (Lecampion et al. 2018).

We discretize the elasticity equations using the displacement discontinuity method (Crouch and Starfield 1983, Bonnet M. 1995) with piece-wise linear element (Crawford and Curran 1982). Because of the singular nature of the elastic kernel, the integral equation is collocated at points inside the displacement discontinuity segments. Knowing the effect in terms of traction of a single piece-wise linear displacement discontinuity, the problem reduces to the one of determining the distribution of displacement discontinuities that generates tractions along the fault such that equilibrium with initial tractions and the failure criterion is satisfied (Crouch and Starfield 1983). The fluid flow equation combining fluid mass conservation and Darcy's law is discretized via a vertex centered finite volume scheme. The fluid pore-pressure is assumed to vary continuously and linearly between element vertex.

In all the simulations reported here, the fault is discretized by N straight equal-sized elements (of size h) - with a total mesh extent of $20 \times a_w$. We therefore have $2N_a$ unknown shear displacement discontinuities (more precisely the plastic multiplier) for the N_a active elements (where , and $N+1$ unknowns for pore-pressure for all the element in the grid. After discretization, we obtain a non-linear system of size $2N_a + N + 1$, whose

unknowns are composed of the plastic multipliers λ (which are linked to increment of slip $\Delta\delta$ through equation (8)) in the N_a active yielded elements, and increment of fluid pressure Δp at every nodes of the grid ($N+1$ unknowns). The size of such a non-linear system evolves with the shear crack propagation as more elements yield mechanically. The non-linearities of such a system are related to shear induced dilatancy and frictional weakening. For a given set of active elements, we use a fixed point iterative scheme to solve for this non-linear system - ending iterations when subsequent estimates of both the increment of slip and pore-pressure are within a relative tolerance of 10^{-6}.

The yielding/active set of element is then re-checked using the Mohr-Coulomb criteria. It is worth noting that an element is at failure when the Mohr-Coulomb criteria is reached for both collocation points in the piece-wise linear displacement discontinuity element.

Over one time-step, such a fully implicit algorithm thus solves the coupled problem by means of two nested loops. The outer loop identify the shear crack position by enforcing implicitly the friction weakening Mohr-Coulomb criterion (3) along the whole fault. The inner loop solve the aforementioned coupled non-linear hydro-mechanical system of equations for a trial set of active/yielded elements.

For numerical efficiency, the time step is adjusted based on the current crack velocity v^n, which is calculated via finite difference:

$$\Delta t^{n+1} = \zeta \frac{h}{v^n}, \tag{28}$$

where h is the element size and ζ is a user-defined constant parameter. This allows to better capture the response of the system during high slip rate, and increase time-step size during slow a-seismic growth. However, a constraint is required to avoid a too small time step that would necessarily occur when the shear crack is approaching a dynamic instability, for which the slip rate and crack velocity diverge. Notably, in our simulation, if the variation is such that $\Delta t^{n+1} < 0.8\Delta t^n$, we set $\Delta t^{n+1} = 0.8\Delta t^n$. Similarly, time-step should remain reasonable in order to avoid sampling the pore pressure evolution too coarsely. In our simulations, if $\Delta t^{n+1} > 3\Delta t^n$, then the time step change is constrained to $\Delta t^{n+1} = 3\Delta t^n$, and the initial time-step is taken as a small fraction of the characteristic diffusion time scale.

Thanks to the semi-analytical results of Garagash and Germanovich (2012) for the non-dilatant case, we have performed a thorough benchmarking of this numerical solver. Some of these verifications are described in the Supporting Information together with a mesh convergence study. Notably, our mesh convergence study have shown that the mesh size h must be such that at least 15 elements cover the characteristic lengthscale a_w to obtain accurate results (i.e. $h \leq a_w/15$). All the simulations reported herein have been performed with $h = a_w/25$.

4.1 Characteristic scales for dimensionless governing problem

By introducing properly chosen characteristic scales to normalize the governing equations, relevant physical processes can be systematically investigated. As already stated in Section 2.1.2, we follow the scaling of Uenishi and Rice (2003) and Garagash and Germanovich (2012) in order to normalize the elasticity equation (1) and friction weakening Mohr-Coulomb criterion (3). We thus scale the slip δ and the tractions t_i by the slip weakening scale δ_w and the peak fault strength $\tau_p = f_p\sigma'_o$, respectively. By doing so, one can identify the nucleation patch length-scale a_w (see equation (12)), which is used to scale all the spatial variables: half crack length a and longitudinal spatial coordinate x. We scale the time t by the characteristic fluid diffusion timescale $a_w^2/(4\alpha)$. The characteristic scale for the fluid over-pressure, is taken as the in-situ effective normal stress σ'_o. Upon scaling the governing equations with the previous characteristic scales, the normalized solution is given by δ/δ_w, τ/τ_p,

σ/σ'_o, $(p-p_o)/\sigma'_o$ and $2a/a_w$ and is function of only the following four dimensionless parameters (besides space and time):

- normalized injection over-pressure $\Delta P/\sigma'_o$
- dimensionless frictional weakening ratio f_r/f_p
- fault stress criticality τ_o/τ_p at in-situ conditions (prior injection)
- dimensionless dilatancy coefficient $\epsilon_d/(\beta\sigma'_o)$

All the numerical results of the following sections have been obtained and will be presented in dimensionless form. For all simulations, we fix the dimensionless frictional weakening ratio to $f_r/f_p = 0.6$ and explore the effect of the remaining dimensionless parameters: $\Delta P/\sigma'_o$, τ_o/τ_p and $\epsilon_d/(\beta\sigma'_o)$.

5 Dilatant hardening effect on a fault characterized by constant permeability

5.1 Case of unstable fault without dilatancy $\tau_o > \tau_r$

We first investigate numerically the effect of dilatancy on otherwise unstable fault, i.e. for which the in-situ shear stress is larger than the residual shear strength and the nucleation of a run-away dynamic rupture is always expected in the absence of dilatancy. We display the time-evolution of the different variables (crack length, maximum slip) using the square root of dimensionless time $\sqrt{4\alpha t}/a_w$ as the x-axis. Such a choice stems from the fact than the injection is diffusion controlled and $\sqrt{4\alpha t}/a_w$ is directly the ratio between the diffusion front over the nucleation lengthscale.

Figures 4-top-left and 4-top-right display the time evolution of half-crack length and peak slip for different values of the dimensionless dilatancy coefficient $\epsilon_d/(\beta\sigma'_o)$ for the case of a rather critically stressed fault $\tau_o/\tau_p = 0.75$ and a moderate injection over-pressure $\Delta P/\sigma'_o = 0.5$. The theoretical estimate of the critical dilatancy sufficient (27) to stabilize the fault is $\epsilon_{d,c}/(\beta\sigma'_o) = 0.25$ in that particular case. We clearly observe that an increase of dilatancy delays the occurrence of a dynamic rupture (highlighted by a red dot on these plots) for values below the critical dilatancy. However, for values of dilatancy equal or larger than the critical one, no nucleation is observed: the propagation is always aseismic. This can be better observed on the time evolution of crack velocity (Figure 4-bottom), where we see how dilatancy larger than the critical value kills the acceleration preceding the nucleation of a dynamic rupture.

Figure 5 displays the profile along the fault of the fluid over-pressure, friction coefficient, shear slip, effective normal stress and shear fault strength at different times for two distinct values of dilatancy, below and above the critical value. For insufficient dilatancy (left panel on figure 5), although an undrained pore-pressure drop can be seen in the weakening zone close to the crack tip, it is not strong enough to stabilize the fault and the last profiles reported in these plots is right before the nucleation of an unabated dynamic rupture. For this particular case without any dilatancy the nucleation occurs early and is not influenced by residual friction. We see that a dilatancy lower than the critical value delays the occurrence of nucleation which is now occurring when a significant part of the crack is at residual friction. For a value of dilatancy larger than the critical one (right panel on figure 5), the crack growth is always quasi-static. The undrained pore-pressure drops is now well developed and its minimum reaches the critical value $\Delta p_u/\sigma'_o = -\epsilon_{d,c}/(\beta\sigma'_o) = -0.25$ locally at the tip. The local fault re-strengthening can be observed on the corresponding effective normal stress profiles as well as on the

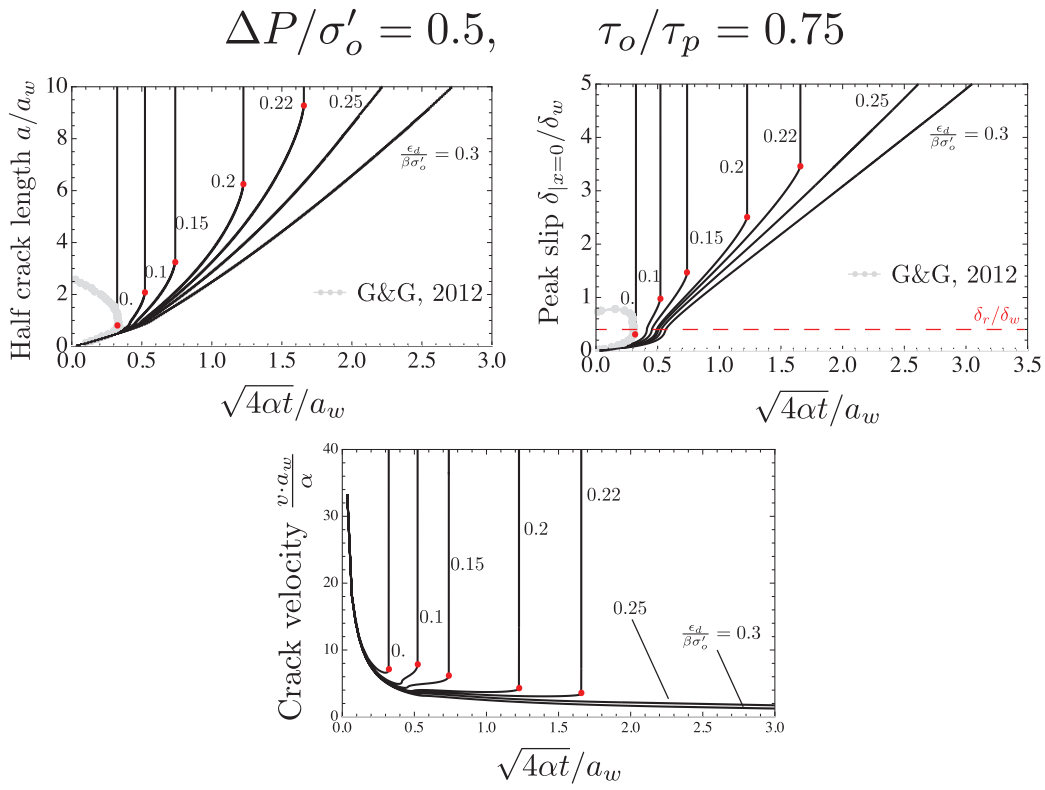

Figure 4: Time evolution of normalized half crack length a/a_w (top-left) and normalized peak slip δ/δ_w at the middle of the fault (top-right), i.e. at $x = 0$, for an otherwise unstable fault ($\tau_o/\tau_p = 0.75$), subjected to moderate over-pressure $\Delta P/\sigma'_o = 0.5$. The friction weakening ratio considered here is $f_r/f_p = 0.6$. The corresponding time evolution of normalized crack velocity va_w/α is showed in the plot at the bottom. We vary the dimensionless dilatancy parameter $\dfrac{\epsilon_d}{\beta\sigma'_o}$ below and above the critical stabilizing value- which is $\epsilon_{d,c}/(\beta\sigma'_o) = 0.25$ in this particular case. Red dots point the onset of unabated dynamic ruptures (color online).

corresponding shear strength versus slip results of our simulation (Figure 5). Under undrained conditions, near the crack tips dilatancy leads to a slip hardening phase before the onset of weakening, a response often observed in healed fault rocks. Brantut and Viesca (2015) used a non-monotonic, piecewise linear slip-dependent strength constitutive law (accounting for a strengthening phase followed by a weakening phase) to investigate earthquake nucleation in healed rocks. They solved semi-analytically an uncoupled problem for which stress perturbation is obtained through a mechanical loading whose time and space dependency is known analytically. They notably show that the strengthening phase that occur before the slip weakening phase considerably increases the critical nucleation size. This is in line with our numerical results for increasing values of dilatancy parameter (see Figure 5-(e) and the crack length at nucleation time for increasing values of dilatancy in Figure 4). We can also observe on these profiles that the weakening zone at the crack tip is small such that the stability condition derived previously under the assumption of small scale yielding is valid.

These simulations confirm the fact that dilatancy can stabilize an otherwise unstable fault if it is above the critical theoretical dilatancy previously derived in section 3.2.2. It is worth noting that this would have been difficult to demonstrate solely numerically even with very long simulations.

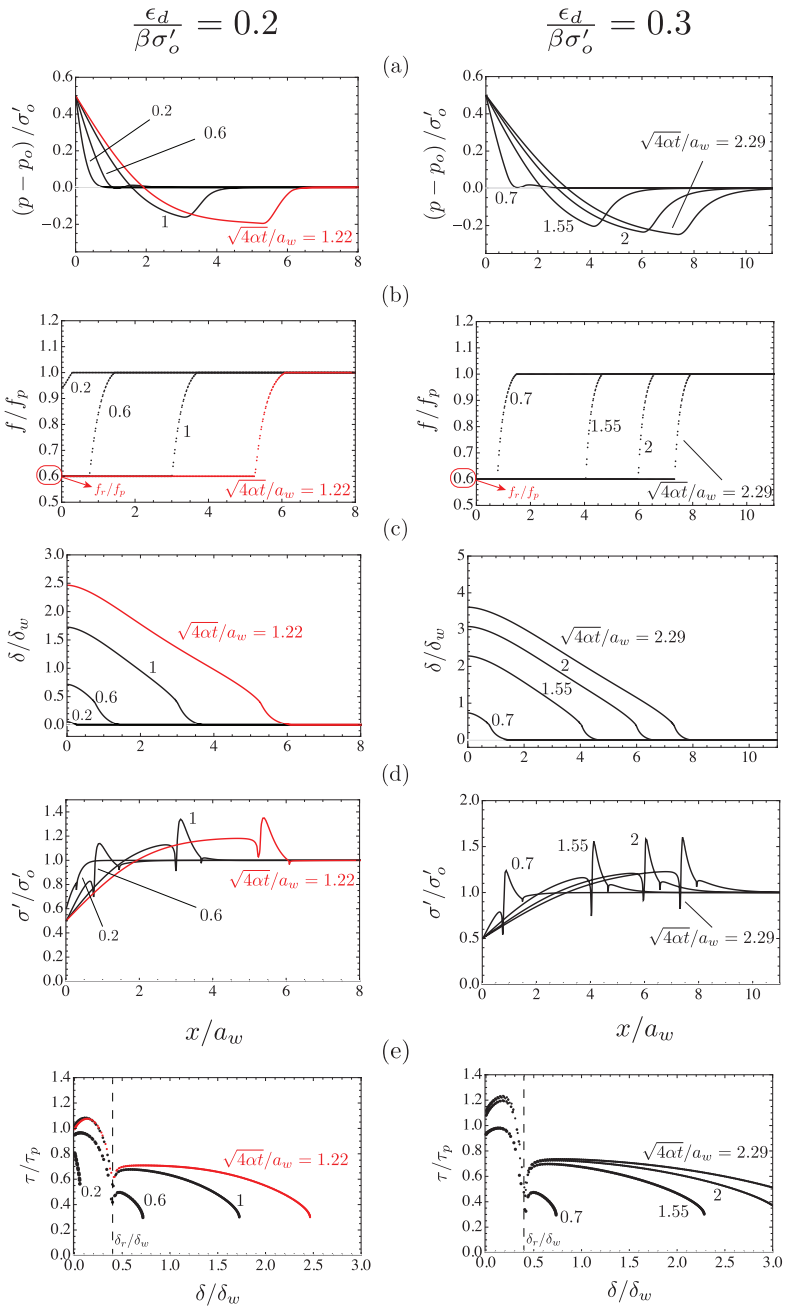

Figure 5: Spatial profile of a) dimensionless pore pressure, b) friction coefficient, c) slip, d) effective normal stress for a critically stressed dilatant fault ($\tau_o/\tau_p = 0.75$), subjected to a moderate overpressure $\Delta p/\sigma'_o = 0.5$, at different (normalized) time snapshots. Sub-figures (e) show the evolution of normalized shear strength with slip, at the same time snapshots. Results for two dimensionless dilatancy parameters are reported: left) ultimately unstable fault for which $\epsilon_d/\beta\sigma'_o$ is lower than the critical stabilizing value for that particular set of parameter ($\epsilon_{d,c}/\beta\sigma'_o = 0.25$), right) ultimately stable for a dimensionless dilatancy above the stabilizing value. Red curves (color online) denote the numerical results at nucleation time for the unstable case (left).

Effect of the injection over-pressure ΔP For the same value of stress criticality $\tau_o/\tau_p = 0.75$, placing ourselves at critical dilatancy ($\epsilon_{d,c}/(\beta\sigma'_o) = 0.25$ in that case), we test the influence of the amount of over-

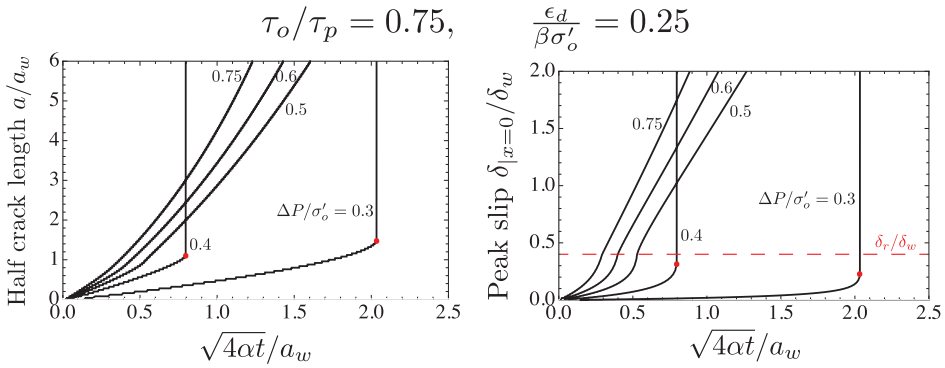

Figure 6: Effect of dimensionless overpressure $\Delta P/\sigma'_o$ on a critically stressed dilatant fault ($\tau_o/\tau_p = 0.75$), in terms of time evolution of dimensionless half crack length a/a_w and dimensionless peak slip $\delta/\delta_{|x=0}$. The dimensionless dilatancy parameter equals the critical value for such configuration: $\epsilon_{d,c}/(\beta\sigma'_o) = 0.25$.

pressure. Figure 6 displays the time evolution of crack length and peak slip for different amount of injection over-pressure ΔP. As expected the larger the injection over-pressure, the faster the crack grows and the propagation remains quasi-static (aseismic). However, an interesting situation occurs for lower value of over-pressures (here $\Delta P/\sigma'_o = 0.4$ and lower) where the nucleation of an unrestricted dynamic rupture is observed. This somehow invalidates the existence of an universal value of stabilizing dilatancy independent of the over-pressure. However, we can clearly see that, for these low over-pressure cases, the peak-slip at the instant of nucleation is lower than the residual slip. In other words, the whole crack is weakening and has not yet reached residual friction. As a result, the undrained pore-pressure is not fully developed and not sufficient to stabilize the fault via dilatant hardening. In these cases, the small scale yielding assumption (small weakening zones at the crack tip) is invalid and the stability condition previously derived for large crack length compared to the characteristic nucleation patch size does not hold. It is worth noting that the nucleation of an unrestricted dynamic rupture is a consequence of the assumption of quasi-static elastic equilibrium. The shear crack velocity at nucleation time diverges instantaneously. Such an unbounded slip rate at nucleation will disappears if inertial terms are accounted for (full elastodynamic or quasi-dynamic formulation): energy dissipation via radiation of elastic waves always ensure a finite crack velocity. In Figure S13 of the Supporting Information, we show that using a quasi-dynamic formulation (with a rather large damping for illustrative purpose) the slip rate remains bounded and the crack propagation eventually slows down at later time compared to the quasi-static formulation where a divergence of the slip rate occurs at nucleation.

In summary, if residual friction is reached during a-seismic crack propagation, the dilatant hardening effect stabilizes the fault for $\tau_r^u > \tau_o$ and the shear crack always propagates quasi-statically. This always occurs for sufficiently large values of over-pressure ΔP, which promotes larger initial aseismic slip rate thus maximizing the effect of dilatant hardening (i.e. sink term associated with dilatancy in the fluid mass conservation (14) is proportional to slip rate - $\tan(\psi(\delta))\frac{\partial \delta}{\partial t}$). On the contrary, a lower over-pressure significantly slows down the initial aseismic crack growth and the beneficial effect of dilatancy can not develop sufficiently to avoid the nucleation of a dynamic rupture even when $\tau_r^u > \tau_o$. If inertia effects are included during crack acceleration (fully dynamic or quasi-dynamic elastic equilibrium), the slip rate will remain bounded and the full effect of dilatant hardening would eventually kick in for sufficient crack length (larger than a_c) - therefore leading to an arrest of the dynamic rupture due to sufficient dilatancy ($\tau_r^u > \tau_o$). Full elastodynamic simulations would be needed to confirm that the dynamic rupture would indeed arrest upon full activation of dilatant hardening

under those conditions of low injection over-pressure and large dilatancy.

For a given set of parameters, the exact minimum value of over-pressure required to fully stabilize the fault can not be estimated analytically, but can be estimated numerically via a series of simulations varying the injection over-pressure. Figure 7 displays such an estimation for different stress criticality τ_o/τ_p below or equal to the undrained residual strength - i.e. the domain where dilatant hardening can stabilize an otherwise unstable fault. More precisely, Figure 7 displays both the maximum overpressure for which a nucleation of finite dynamic event occur and the minimum over-pressure for which the propagation is solely aseismic (the fault is stabilized). A linear increase of the required over-pressure as the stress criticality decreases can be clearly observed. This can again be understood as a larger driving force is required to reach residual friction for lower stress criticality.

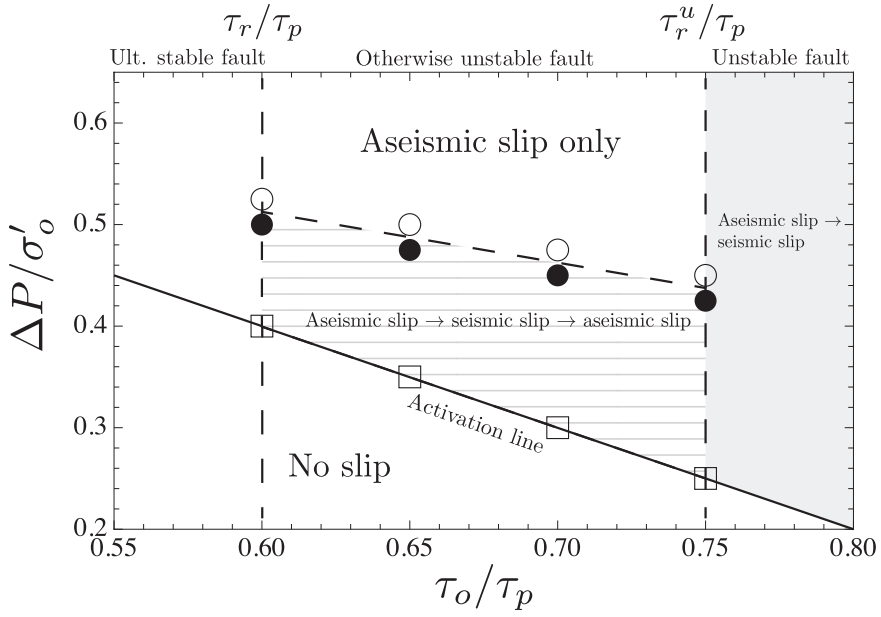

Figure 7: Numerical estimation of the minimum amount of over-pressure required to activate the full benefit of dilatant hardening and stabilize an otherwise unstable fault ($\tau_r < \tau_o$) for different stress criticality between the ultimately stable limit ($\tau_r/\tau_p = f_r/f_p = 0.6$ in that case) and the undrained dilatant residual strength ($\tau_r^u/\tau_p = 1.25\tau_r/\tau_p = 0.75$ in that case). The black filled circle denotes the maximum value of over-pressure below which a finite dynamic event always nucleate (for over-pressure above the slip activation limit), while the empty circle corresponds to the minimum normalized over-pressure required to stabilize such a fault (aseismic slip only for larger over-pressure). The minimum over-pressure required for slip activation ($\Delta P/\sigma'_o = 1 - \tau_o/\tau_p$) is also displayed as empty square/continuous line. Stress criticality τ_o/τ_p larger than τ_r^u/τ_p always result in the nucleation of unrestricted dynamic rupture for any value of over-pressure larger than the activation limit.

5.2 Case of an ultimately stable fault even without dilatancy ($\tau_o < \tau_r$)

We now turn to the case of ultimately stable fault ($\tau_o < \tau_r$), where only a transient seismic episode occurs for moderate over-pressure (region 2 of Figure 3) while crack growth is strictly aseismic for large over-pressure (region 3 of Figure 3).

For a configuration representative of region 2 in Figure 3 ($\tau_o/\tau_p = 0.55, \Delta P/\sigma'_o = 0.5$) a transient seismic episode occurs for a low accumulated slip: the residual friction is not yet reached anywhere in the crack. Such

a seismic event is directly linked with the crack "catching" up the fluid front in association with frictional weakening. Figure 8 displays the crack evolution and peak slip for such configuration for different values of dilatancy. Increasing dilatancy slow down the initial quasi-static crack growth and thus delay the nucleation of this finite seismic slip episode. Interestingly, because with larger dilatancy, the quasi-static crack lags even more behind the fluid diffusion front prior to nucleation, the dynamic run-out increases for larger dilatancy. After this finite seismic slip episode, upon continuous injection, the shear crack propagates quasi-statically on par with the evolution of the diffusion front $a \propto \sqrt{4\alpha t}$. Larger dilatancy slows down the quasi-static crack growth. The corresponding profiles of over-pressure, friction coefficient, slip and effective normal stress along the fault at different time snapshots are reported in Supporting Information (see Figure S6). The finite seismic episode can be clearly seen where we observe that prior to nucleation the weakening zone occupies the whole crack. Because the fault is ultimately stable, beside the seismic episode, the fault propagates quasi-statically: due to the low slip rate, dilatancy does not significantly alter the pore-pressure profile although the effect can be observed on the effective normal stress profiles (see Supporting Information, Figure S6).

Finally for large over-pressure (region 3 of Figure 3), the crack growth is always quasi-static (aseismic). Results for such aseismic growth are reported in Supporting Information. For similar stress and fault strength conditions, an increase of the fault dilatancy slows down the crack velocity as expected.

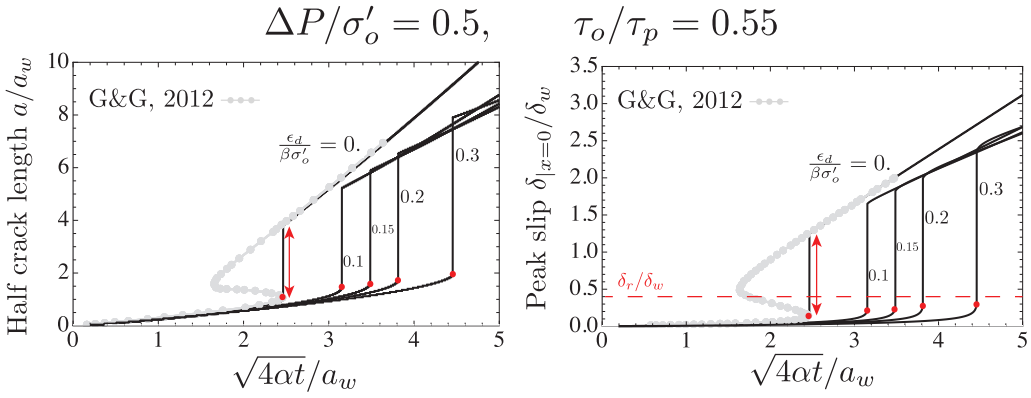

Figure 8: Time evolution of normalized half crack length a/a_w and normalized peak slip δ/δ_w at the middle of the fault, i.e. at $x = 0$, for an ultimately stable fault ($\tau_o/\tau_p = 0.55$ and $\tau_o < \tau_r$, for $f_r/f_p = 0.6$), subjected to moderate over-pressure $\Delta P/\sigma'_o = 0.5$. We span several dilatancy cases by varying the dimensionless dilatancy parameter $\epsilon_d/(\beta\sigma'_o)$. Red dots denote the onset of dynamic event, which is always characterized by a nucleation followed by an arrest (red arrow). The run-out distance increases with increase values of dimensionless dilatancy parameter $\epsilon_d/\beta\sigma'_o$.

6 Effect of shear-induced permeability changes

The results presented so far are based on the assumption of a constant fault permeability - although in our numerical results the fault transmissivity $w_h k_f$ is changing in conjunction with the dilatant behavior. Experimental (Makurat et al. 1985, Lee and Cho 2002, Li et al. 2008, e.g.) and field evidences (Evans et al. 2005a,b) have shown that deep fractures under fluid induced slip exhibit an increase of fault permeability (Cornet 2015, Evans et al. 2005a,b, McClure and Horne 2014). It is important to note that, although possibly significant, the increase of permeability with slip remains small compared to the drastic increase observed when the fracture

opens (i.e. when the effective normal stress becomes tensile) such as in hydraulic fracturing. Like previously, we restrict here to the case of compressive effective normal stress, where permeability changes with slip are strictly associated with shear-induced dilatancy.

Several empirical models have been proposed and used in literature for permeability evolution. Some of them account for porosity changes, while some others include explicit dependency on effect stress changes (see e.g. (Rutqvist and Stephansson 2003) for a review). For example, Rice (1992) used an effective stress-dependent permeability law, in which the permeability is a non-linearly decreasing function of the local (compressive) effective normal stress:

$$k_f = k_* e^{\left(-\sigma'/\sigma_*\right)}, \tag{29}$$

where k_* is the maximum fault permeability $\left[L^2\right]$ and σ_* is a normalizing stress level $\left[ML^{-1}T^{-2}\right]$ which ranges between 3 to 40 MPa Rice (1992) - see also (Seront et al. 1998). Another common choice is to use the cubic law for the fault transmissivity ($k_f w_h$), relating the fault permeability directly to the changes of aperture - i.e. a parallel plate idealization of the fluid flow in the fault (Bawden et al. 1980, McClure and Horne 2014, Ucar et al. 2018, e.g.):

$$k_f\left(\delta\right) = \frac{w_h\left(\delta\right)^2}{12} \tag{30}$$

Under this assumption, the maximum constant fault permeability that is exerted when the slip δ is larger than the critical value δ_r is directly function of dilatant strain ϵ_d as $k_{f,max} = \frac{\omega_o^2}{12}(1+\epsilon_d)^2$. Such a maximum increase of longitudinal permeability with respect to its initial value $\omega_o^2/12$ is actually rather small since the dilatant strain ϵ_d ranges between $10^{-4} - 10^{-2}$. This is clearly in contradiction with experimental and field evidences which mention much larger permeability increase (Makurat et al. 1985, Evans et al. 2005a,b).

In order to investigate cases in which fault dilatancy induces significant increases of fault permeability with inelastic deformations (for instance due to change of fault porosity, for which $\Delta k_f \propto \Delta\varphi^{7-8}$ for dense rocks - see Bernabé et al. (2003)), we generalize the fault permeability evolution law as

$$k_f = \frac{\omega_o^2}{12}\left(1 + a\frac{w(\delta)}{\omega_o}\right)^b, \tag{31}$$

where a and b are two constant parameters. Note that when $a = 1$ and $b = 2$, the fault transmissivity obeys the cubic law. By varying these two parameters, one can obtain ten-fold permeability increase associated with shear slip at maximum dilatancy compared to the initial value $\omega_o^2/12$. We use this permeability law (31) to gauge the impact of permeability change with slip on the stabilization by dilatancy of an otherwise unstable fault. In particular, our aim is to see if an increase of permeability affect the stabilizing effect of the undrained pore pressure drop associated with dilatancy.

We focus on the case of an otherwise unstable fault $\tau_o/\tau_p = 0.75$ ($f_r/f_p = 0.6$) and a moderate over-pressure case $\Delta P = 0.5$ with a dilatancy equal to the critical stabilizing value $\epsilon_{d,c}/(\beta\sigma'_o) = 0.25$ for these conditions. Figure 9 displays the crack length and peak slip evolution for the case of a constant permeability as well as for different values of a and b for the permeability evolution law (31). We span $a = 1$, $b = 2$ (cubic law) and $a = 2$, $b = 3$, 5, 8, and 10 which entails respectively a 1.5 (cubic law), 3.3, 7.6, 25.6 and 57.6 fold increases of permeability at maximum dilatancy.

We observe that although the increase of permeability directly enhance the crack velocity, the propagation always remains aseismic. The permeability increase has a very significant effect on aseismic growth and this effect increases with the value of b as expected. For example, for the strongest permeability variation with dilatancy ($a = 2$, $b = 10$ resulting in $k_{f,max}/k_{fo} \sim 57.6$), we observe a $\sim 550\%$ increase in crack length at $\sqrt{4\alpha t}/a_w = 0.27$ compared to the constant permeability case (see Figure 9). A difference that will obviously

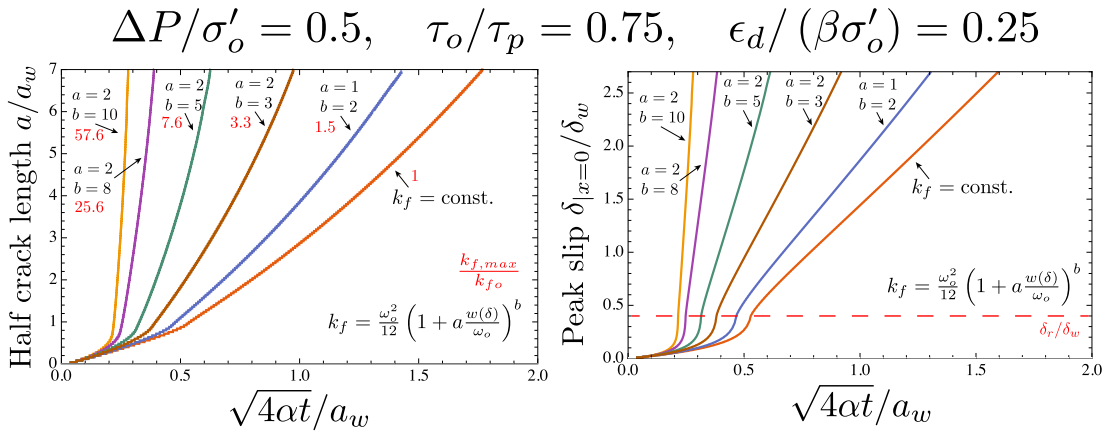

Figure 9: Effect of permeability increase on a critically stressed ($\tau_o/\tau_p = 0.75$, $f_r/f_p = 0.6$) dilatant fault under moderate over-pressure ($\Delta P/\sigma'_o = 0.5$): time evolution of normalized half crack length a/a_w and corresponding peak slip $\delta_{|x=0}/\delta_w$. The dimensionless dilatancy parameter $\epsilon_d/(\beta\sigma'_o)$ is set to the corresponding critical stabilizing value (27), equal here to 0.25. The effect of permeability evolution following the slip dependent law (31) is investigated for five different values of the parameters (a, b) spanning small and large permeability increase from 1.5 to ~ 60 times the initial fault permeability.

continue to grow with time. For such a evolution of permeability with slip (31), the permeability profile is similar to the dilatancy strain: constant at is maximum value all along the crack except in the weakening zone near the tip - see Figure S10 in Supporting Information. The large permeability increases with slip, however, do not modify the stabilizing effect of undrained dilatant hardening. As the permeability accelerates quasi-static crack growth, the undrained pore-pressure response remains strong at the crack tip (see the pore-pressure profiles in Figure S10 in Supporting Information)Moreover, due to the quasi-static acceleration with increasing permeability, residual friction is reached earlier such that the undrained shear strength is fully mobilized - even possibly for smaller value of over-pressure compared to the constant permeability case. Note that similar results are obtained with other type of permeability evolution (such as the one described by eq.(29)) as reported in Figures S11 and S12 of the Supporting Information. In conclusions, in the case of an impermeable surrounding, the increase of permeability with slip along the fault does not affect the ultimate stability condition ($\tau_o < \tau_r^u$).

7 Conclusions

We have investigated the effect of dilatancy on the transition from seismic to aseismic slip due to sustained fluid injection regulated at a constant pressure in a fault. Although simple in its nature (planar bi-dimensional fault, uniform in-situ stress and rock properties, linear weakening friction), the model investigated properly couples, via non-associated plasticity, the hydro-mechanical interplay between slip, dilatancy, frictional weakening and fluid flow. We have developed a robust fully implicit numerical scheme - which properly reproduces existing semi-analytical solutions for the case of non-dilatant fault (Garagash and Germanovich 2012). We notably would like to emphasize the necessity of numerical model verification for such type of non-linear fracture propagation problem which -similarly to hydraulic fracturing problem- necessitates to resolve multiple scales (weakening zone and diffusion lengthscale here).

We have shown that dilatant hardening can stabilize an otherwise unstable fault ($\tau_o > \tau_r$), as long as the

weakening of friction occurs in a small zone near the tip of the shear crack (small scale yielding). This is captured by an ultimate stability condition defined with an undrained residual strength $\tau_r^u = \tau_r(1+\epsilon_d/(\beta\sigma'_o))$ function of the dilatant strain of the fault at critical state (when dilatancy saturates). We have demonstrated theoretically that under the assumption of small scale yielding, dilatancy ultimately stabilize the fault if $\tau_o < \tau_r^u$. In other words, for a given fault criticality, there exists a critical dilatancy above which the fault will remain stable and shear slip is solely aseismic. However, the hypothesis behind small scale yielding (small frictional weakening zone near the crack tips) must be satisfied for such a ultimate stability condition to hold. This is the case if and only if the injection over-pressure is sufficient to propagate quasi-statically the shear crack / slipping patch fast enough to reach residual friction and activate the beneficial effect of dilatancy prior to the crack reaching the nucleation length of the non-dilatant case. For injection pressures below a limiting value, the crack propagates too slowly initially. The nucleation of a dynamic rupture occurs prior to reaching residual friction such that the maximum dilatancy is not activated prior to nucleation. For such small injection over-pressure, dilatancy cannot prevent the nucleation of a dynamic rupture for an unstable fault ($\tau_o > \tau_r$) even for large dilatancy $\tau_o < \tau_r^u$ (see Figure 7 for the evolution of the minimum overpressure). However, such a dynamic rupture for low over-pressure and a-priori sufficient dilatancy ($\tau_o < \tau_r^u$) - which occurs prior to reaching residual friction - will eventually arrest as the dilatant hardening effect kicks in for sufficient crack length. Although observed with quasi-dynamic damping (see Supplemental Information), a fully elastodynamics simulation would be required to confirm such arrest.

For an ultimately stable fault ($\tau_o < \tau_r$), our numerical results indicate that dilatancy delays the occurrence of a finite episode of dynamic slip for moderate overpressure. Such a finite seismic event is associated with the abrupt catch up of the diffusion front by the crack front and the fact that the residual friction has not yet reached all along the crack. For large over-pressure and stable fault, an increasing dilatant behavior simply slows down the quasi-static propagation (strictly aseismic slip).

Permeability increases with slip leads to faster aseismic crack growth for the different permeability evolution tested. However, it does not affect the critical dilatancy stabilizing an otherwise unstable fault. It appears evident that the details of the slip-permeability law greatly influence aseismic growth - a discussion on the most appropriate permeability model clearly require more investigation and necessarily better controlled hydro-mechanical laboratory experiments for sufficient slippage length.

The strengthening effect of dilatancy discussed here must be put perspective with some well-known dynamic weakening mechanisms that may occur as the crack accelerates: notably, thermal pressurization and flash heating of asperities. Although the effect of these weakening mechanisms have been already studied (Garagash and Rudnicki 2003, Segall and Rice 2006, Rice 2006, Garagash and Germanovich 2012) in the scope of earthquake nucleation via remote loading, a complete investigation of such competition would be required in the context of fluid injection. This is out of the scope of this paper. We note however that both of these dynamic weakening mechanisms requires dynamic slip rates (m/s and above) while dilatant hardening is activated quasi-statically. A probably more important point with respect to the stabilizing effect of dilatant hardening is related to the assumption of an impermeable host rock. Although possibly acceptable for young fault/fractures, this is highly doubtful for most mature fault structure. With a permeable surrounding (of say hydraulic diffusivity α_r), the undrained pore-pressure drop associated with the fault dilatant behavior may be short-lived as fluid will be sucked in the fault and re-pressurize it. The importance of dilatant hardening will directly depend on the ratio between the changes due to dilatancy (which scales with slip rate) and the influx of fluid from the rock mass (which scales as α_r/h_w with $h_w \approx \omega_o$ the gouge thickness). A thorough investigation for the case of injection induced slip is required to clarify that competition further, along the lines of Segall and Rice (1995), Segall et al.

(2010) in the context of the seismic cycle. In the sequel, we have also used a simple linear weakening friction law compared to a more elaborate rate-state model. It is nevertheless worthwhile to note that some work (Uenishi and Rice 2003, Viesca 2016a,b) have demonstrated a correspondence between linear weakening friction and rate and state at the onset of nucleation. Investigations of the combined effect of rate and state and dilatancy in the case of fluid injection combined with proper scaling and stability analysis would surely produce a more refined understanding of the mechanisms of induced seismicity.

Finally, we conclude by recalling the decreases of dilatancy with confinement, such that the effect of dilatant hardening is likely to be more prominent mostly at shallow depths. Additional experimental data of fault dilatant behavior in conjunction with frictional properties would enable to further decipher its impact on fluid induced a-seismic and seismic slip with the help of the type of model presented here.

Acknowledgments This work was funded by the Swiss Federal Office of Energy (Stim-Design project, SI/501354-01) and the Swiss National Science Foundation under grant 160577.

References

JH Healy, WW Rubey, DT Griggs, and CB Raleigh. The denver earthquakes. *Science*, 161(3848):1301–1310, 1968.

D. H. Hamilton and R. L. Meehan. Ground Rupture in the Baldwin Hills. *Science*, 172:333–344, 1971.

O. Scotti and F. H. Cornet. In Situ Evidence for Fluid-Induced Aseismic Slip Events Along Fault Zones. *Int. J. Rock Mech. Min. Sci. & Geom. Abstr.*, 31(4):347–358, 1994.

F. H. Cornet, J. Helm, H. Poitrenaud, and A. Etchecopar. Seismic and Aseismic Slips Induced by Large-scale Fluid Injections. *Pure and Applied Geophysics*, 150:563–583, 1997.

S. A. Shapiro, J. Kummerow, C. Dinske, G. Asch, E. Rothert, J. Erzinger, H.-J. Kumpel, and R. Kind. Fluid induced seismicity guided by a continental fault: Injection experiment of 2004/2005 at the German Deep Drilling Site (KTB). *Journal of Geophysical Research*, 33, 2006.

W. L. Ellsworth. Injection-induced earthquakes. *Science*, 341, July 2013.

Robert J Skoumal, Michael R Brudzinski, and Brian S Currie. Earthquakes induced by hydraulic fracturing in poland township, ohio. *Bulletin of the Seismological Society of America*, 105(1):189–197, 2015.

X. Bao and D. W. Eaton. Fault activation by hydraulic fracturing in western Canada. *Science*, 2016.

F.E. Cornet. *Elements of Crustal Geomechanics*. Cambridge University Press, 2015.

D. I. Garagash and L. N. Germanovich. Nucleation and arrest of dynamic slip on a pressurized fault. *J. Geophys. Res.*, 117, 2012.

Y. Guglielmini, F. Cappa, J.-P Avouac, P. Henry, and D. Elsworth. Seismicity triggered by fluid injection-induced aseismic slip. *Science*, 348, June 2015.

S. Wei, J.-P Avouac, K. W. Hudnut, A. Donnellan, J. W. Parker, R. W. Graves, D. Helmberger, E. Fielding, Z. Liu, F. Cappa, and M. Eneva. The 2012 Brawley swarm triggering by fluid-induced aseismic slip. *Earth and Planetary Science Letters*, 442:115–125, 2015.

F. H. Cornet. Seismic and aseismic motions generated by fluid injections. *Geomechanics for Energy and the Environment*, 5:42–54, 2016.

P. Segall and J. R. Rice. Dilatancy, compaction, and slip instability of a fluid-infiltrated fault. *Journal of Geophysical Research*, 100(B11):22,155–22,171, 1995.

P. Segall, A. M. Rubin, A. M. Bradley, and RI. Dilatant strengthening as a mechanism for slow slip events. *Journal of Geophysical Research*, 115(B12305), 2010.

J. W. Rudnicki and C-H. Chen. Stabilization of rapid frictional slip on a weakening fault by dilatant hardening. *Journal of Geophysical Research*, 93(B5):4745–4757, May 10 1988.

D. A. Lockner and J. D. Byerlee. Dilatancy in hydraulically isolated faults and the suppression of instability. *Geophysical Research Letters*, 21(22):2353–2356, 1994.

J. Samuelson, D. Elsworth, and C. Marone. Shear-induced dilatancy of fluid-saturated faults: Experiments and theory. *Journal of Geophysical Research*, 114, 2009.

AS Batchelor and Stubs. Hot dry rock reservoir stimulation in the UK an extended summary. In *International seminar on the results of EC geothermal energy research. 3*, pages 681–711, 1985.

J. R. Rice. On the stability of dilatant hardening for saturated rock masses. *Journal of Geophysical Research*, 80(11), 1975.

Rudnicki, J. W. The stabilization of slip on a narrow weakening fault zone by coupled deformation-pore fluid diffusion. *Bull. Seism. Soc. Am.*, 69(4):1011–1026, 1979.

B. Shibazaki. Nucleation process with dilatant hardening on a fluid-infiltrated strike-slip fault model using a rate- and state-dependent friction law. *Journal of Geophysical Research*, 110(B11308), 2005.

R. Viesca and J. R. Rice. Nucleation of slip-weakening rupture instability in landslides by localized increase of pore pressure. *Journal of Geophysical Research*, 117(B03104), 2012.

X. Zhang, R. G. Jeffrey, and E. M. Llanos. On plane-strain fluid-driven shear fracture propagation in elastic solids. *Geophys. J. Int.*, 163:419–430, 2005.

Y. Ida. Cohesive force across the tip of a longitudinal-shear crack and griffith's specific surface energy. *Journal of Geophysical Research*, 77(20):3796–3805, 1972.

J. R. Rice. *Mathematical analysis in the mechanics of fracture*, volume 2, chapter Fracture: An Advanced Treatise, pages 191–311. Academic Press, 1968.

A. C. Palmer and J. R. Rice. The growth of slip surfaces in the progressive failure of over-consolidated clay. In *Proc. Roy. Soc. Lond.*, volume 332, pages 527–548, 1973.

M. Gebbia. Formule fondamentali della statica dei corpi elastici. *Rend. Circ. Mat. di Palermo*, 5:320–323, 1891.

S. L. Crouch and A. M. Starfield. *Boundary Element Methods in Solid Mechanics*. George Allen and Unwin, 1983.

D. A. Hill, P.A Kelly, D.N Dai, and A. M. Korsunsky. *Solution of Crack Problems: the Distributed Dislocation Technique*, volume 44. Kluwer Academic Publishers, 1996.

J. R. Rice. Spatio-temporal complexity of slip on a fault. *Journal of Geophysical Research*, 98(B6):9885–9907, June 1993.

Lubliner, J. *Plasticity Theory*. Dover, 2005.

G. Maier, G. Novati, and Z. Cen. Symmetric galerkin boundary element method for quasi-brittle-fracture and frictional contact problems. *Computational Mechanics*, 13:74–89, 1993.

J. C. Simo and T.J.R. Hughes. *Computational Inelasticity*, volume 7. Springer, 1997.

K Matsuki, Y Kimura, K Sakaguchi, A Kizaki, and AA Giwelli. Effect of shear displacement on the hydraulic conductivity of a fracture. *International Journal of Rock Mechanics and Mining Sciences*, 47(3):436–449, 2010.

N. Barton, S. Bandis, and K. Bakhtar. Strength, deformation and conductivity coupling of rock joints. *Int. J. Rock Mech. Min. Sci. & Geom. Abstr.*, 22(3):121–140, 1985.

Chris Marone, C Barry Raleigh, and CH Scholz. Frictional behavior and constitutive modeling of simulated fault gouge. *Journal of Geophysical Research: Solid Earth*, 95(B5):7007–7025, 1990.

K. Uenishi and J. R. Rice. Universal nucleation length for slip-weakening rupture instability under nonunifrom fault loading. *Journal of Geophysical Research*, 108(B1), 2003.

H. Lockner, D.and Naka, H. Tanaka, H. Ito, and R. Ikeda. Permeability and Strength of core samples from the Nojima fault of the 1995 Kobe earthquake. In *Int. workshop on the Nojima fault core and borehole data analysis*, 1999.

H. S. Carslaw and J. C. Jaeger. *Conduction of heat in solids*. Oxford at the clarendon press, 1959.

H. Tada, P. C. Paris, and G. R. Irwin. *The Stress Analysis of Crack Handbook*. ASME Press, 3rd edition, 2000.

A. Quarteroni, R. Sacco, and F. Saleri. *Numerical Mathematics*. Texts in applied mathematics. Springer, 2000.

B. Lecampion, A. P. Bunger, and X. Zhang. Numerical methods for hydraulic fracture propagation: A review of recent trends. *Journal of Natural Gas Science and Engineering*, 49:66–83, 2018.

Bonnet M. . *Boundary Integral Equation Methods for Solids and Fluids*. John Wiley and Sons Ltd, 1995.

A. M. Crawford and J. H. Curran. Higher-order functional variation displacement discontinuity elements. *Int. J. Rock Mech. Min. Sci. & Geom. Abstr.*, 19(3), 1982.

N. Brantut and R. C. Viesca. Earthquake nucleation in intact or healed rocks. *Journal of Geophysical Research: Solid Earth*, 120:191–209, 2015.

A Makurat, SP Neuman, and ES Simpson. The effect of shear displacement on the permeability of natural rough joints. *Hydrogeology of rocks of low permeability: International Association of Hydrogeologists Memoir*, 17:99–106, 1985.

H. S. Lee and T. F. Cho. Hydraulic Characteristics of Rough Fractures in Linear Flow under Normal and Shear Load. *Rock Mech. Rock Engng.*, 35(4):299–318, 2002.

Bo Li, Yujing Jiang, Tomofumi Koyama, Lanru Jing, and Yoshihiko Tanabashi. Experimental study of the hydro-mechanical behavior of rock joints using a parallel-plate model containing contact areas and artificial fractures. *International Journal of Rock Mechanics and Mining Sciences*, 45(3):362–375, 2008.

K.F. Evans, A. Genter, and J. Sausse. Permeability creation and damage due to massive fluid injections into granite at 3.5 km at soultz: 1. borehole observations. *Journal of Geophysical Research: Solid Earth*, 110(4): 1–19, 2005a.

K. F. Evans, H. Moriya, H. Niitsuma, R. H. Jones, W. S. Phillips, A. Genter, J. Sausse, R. Jung, and R. Baria. Microseismicity and permeability enhancement of hydrogeologic structures during massive fluid injections into granite at 3 km depth at the Soultz HDR site. *Geophys. J. Int.*, 160:388–412, 2005b.

M. W. McClure and R. N. Horne. An investigation of stimulation mechanisms in Enhanced Geothermal Systems. *Int. J. Rock Mech. Min. Sci.*, 72:242–260, 2014.

J. Rutqvist and O. Stephansson. The role of hydrochemical coupling in fractured rock engineering. *Hydrogeology Journal*, 11(1):7–40, 2003.

J. R. Rice. Fault Stress States, Pore Pressure Distributions, and the Weakness of the San Andreas Fault. *International Geophysics*, 51:475–503, 1992.

B. Seront, T.-F. Wong, J.S. Caine, C.B. Forster, R.L. Bruhn, and J.T. Fredrich. Laboratory characterization of hydromechanical properties of a seismogenic normal fault system. *Journal of Structural Geology*, 20(7): 865–881, 1998.

W. F. Bawden, J. H. Curran, and J.-C. Roegiers. Influence of Fracture Deformation on Secondary - A Numerical Approach. *Int. J. Rock Mech. Min. Sci. & Geom. Abstr.*, 17:265–279, 1980.

E. Ucar, I. Berre, and E. Keilegavlen. Three-Dimensional Numerical Modeling of Shear Stimulation of Fractured Reservoirs. *Journal of Geophysical Research*, 123:3891–3908, 2018.

Y. Bernabé, U. Mok., and B. Evans. Permeability-porosity Relationships in Rock Subjected to Various Evolution Processes. *Pure and Applied Geophysics*, 160:937–960, 2003.

D. I. Garagash and J. W. Rudnicki. Shear heating of a fluid-saturated slip-weakening dilatant fault zone, 1, limiting regimes. *J. Geophys. Res.*, 108(B2), 2003.

P. Segall and J. R. Rice. Does shear heating of pore fluid contribute to earthquake nucleation? *Journal of Geophysical Research: Solid Earth*, 111(B9), 2006.

J. R. Rice. Heating and weakening on faults during earthquake slip. *J. Geophys. Res*, 111(B05311), 2006.

Robert C Viesca. Stable and unstable development of an interfacial sliding instability. *Physical Review E*, 93 (6):060202, 2016a.

Robert C Viesca. Self-similar slip instability on interfaces with rate-and state-dependent friction. *Proc. Roy. Soc. Lond. A*, 472(2192):20160254, 2016b.